# Ligand dynamics and reactivity of a non-innocent homoleptic iron complex (N,N)₂Fe stabilized by phen-type ligands

Mae Féo,[a] Faycel Djebbar,[a] Fedor Zhurkin,[a] Laurent Binet,[b] Nadia Touati,[b] Matthew C. Leech,[c] Kevin Lam,[c] Eric Brémond[d] and Guillaume Lefèvre*[a]

[a] Chimie ParisTech – PSL, UMR 8060 i-CleHS, CNRS, 11 rue Pierre et Marie Curie, 75005 Paris, FR, guillaume.lefevre@chimieparistech.psl.eu
[b] ChimieParisTech, Université PSL, CNRS, Institut de Recherche de Chimie-Paris (IRCP), PCMTH, 75005 Paris, France
[c] School of Science, Faculty of Engineering and Science, University of Greenwich, Chatham Maritime, Kent, ME4 4TB, UK
[d] Université Paris Cité, ITODYS, CNRS, F- 75013 Paris, France
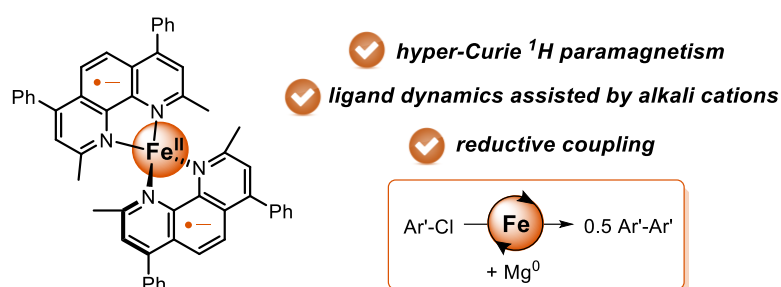
**Keywords**

Iron catalysis, NMR, paramagnetism, cycloaddition, reductive coupling

**Abstract**

We report in this work the spectroscopic and reactivity properties of a non-innocent paramagnetic iron complex $(bcp^{\bullet-})_2Fe^{II}$ featuring formally a $Fe^0$ center stabilized by two bathocuproine (bcp) ligands. The origin of the paramagnetic $^1H$ NMR behavior is analyzed by means of DFT calculations, and shows that two electronic states of the complex contribute to its spectroscopic properties. The dynamics of the coordination sphere in $(bcp^{\bullet-})_2Fe^{II}$ is governed by the duality between the two electronic descriptions $(bcp^{\bullet-})_2Fe^{II}$, and $(bcp)_2Fe^0$. The strong antiferromagnetic coupling between the reduced bcp scaffolds and the ferrous ion in $(bcp^{\bullet-})_2Fe^{II}$ makes substitution of the $bcp^{\bullet-}$ ligand difficult; however, the reduced $(bcp)_2Fe^0$ character allows substitution of bcp by π-accepting ligands, such as alkynes, which can be activated in catalytic cycloadditions with the assistance of main-group salts. $(bcp^{\bullet-})_2Fe^{II}$ also shows reductive activity towards a variety of organic electrophiles, and preliminary results using this complex as a catalyst for the reductive coupling of heteroaryl chlorides are discussed.

# 1. Introduction

Phenanthroline-type ligands (phen) are ubiquitous in coordination chemistry and the associated complexes have been broadly used and investigated for decades. Due to the easy functionalization of this scaffold, such complexes still witness recent applications. Phenanthroline-containing transition-metal-complexes indeed display a large variety of properties, with possible applications in photochemistry, catalysis, or analytical chemistry.[1-3] In the particular field of iron organometallic chemistry, the iron-phen coordination patterns are largely dominated by the $Fe^{II}$ and $Fe^{III}$ oxidation states, and well-defined complexes featuring a formally reduced iron center (that is, with an oxidation state lower than +II) are extremely scarce.

Due to the low-lying LUMO levels of the phen scaffold, those complexes display a non-innocent behavior, and an electron transfer from the metal onto the $\pi^*$ system of the ligand occurs. More generally, the association of formally reduced iron complexes with non-innocent ligands has been described and used by Chirik with pyridinediimine ligands,[4-5] as well as by Gordon and Trovitch for 2,2'-bipyridine (bpy) ligand,[6] but the examples of well-defined reduced iron complexes involving a ligation by phen-type ligands are rare. The lack of well-defined coordination chemistry of phen ligands associated to low oxidation states originates in the intrinsic instability of the non-innocent species which are generated under those conditions. Singly- or doubly-reduced phenanthrolines indeed exhibit a strong reducing activity, and therefore mostly act as reduction catalysts as a relay in electron transfer steps,[7] often precluding their structural characterization as reduced ligands in non-innocent platforms. Upon reduction of the phen scaffold, several positions of the latter can acquire a radical character, as showed for example by the LUMO+1 level of the phen (Scheme 1a).
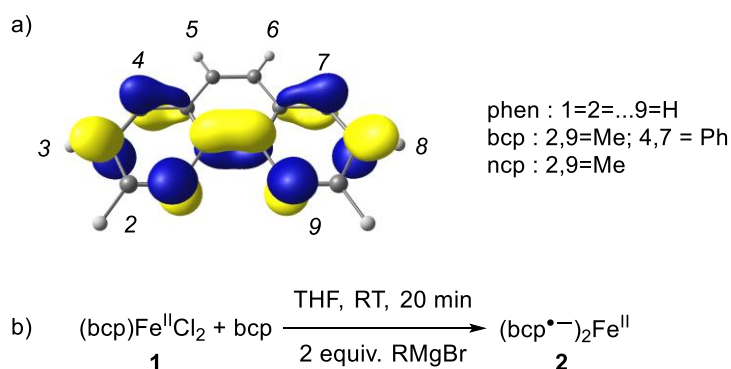


Scheme 1 : a) DFT-computed LUMO+1 level of phen; b) synthesis of $(bcp^{\bullet-})_2Fe^{II}$ by reduction of **1** with a Grignard reagent; R = Et or $Me_2C=CH$.

We recently demonstrated that the $(bcp)Fe^{II}Cl_2$ precursor (**1**), where bcp is the bathocuproine ligand (Scheme 1a) could be efficiently reduced into a neutral $(bcp)_2Fe$ complex (**2**, Scheme 1b). This complex proved to be non-innocent, featuring two singly-reduced $bcp^{\bullet-}$ anions antiferromagnetically coupled to a high-spin $Fe^{II}$ ion, leading to a $(bcp^{\bullet-})_2Fe^{II}$ platform.[8] A similar complex, involving ligation by neocuproine ligand (ncp, Scheme 1a) was characterized by Anderson, and also displayed a similar non-innocent structure $(ncp^{\bullet-})_2Fe^{II}$ (**2'**).[9]

Albeit structurally close, complexes **2** and **2'** display drastically different thermal and kinetic stabilities. Substitution of C4 and C7 positions of the phen scaffold by Ph groups in bcp led to a more stable reduced complex **2**, the unsubstituted analogue **2'** described by Anderson [9] and involving neocuproine (ncp) ligation following decomposition pathways at much lower temperatures and shorter reaction times. This better stability of the bcp complex **2** has been attributed to the steric protection brought by the phenyl

groups at the C4/C7 positions, which display a marked C-centered radical character. This steric hindrance thus helps to hamper the decomposition of the reduced bcp scaffold by classic radical pathways (dimerization, as described by Nocton in the case of phen-rare-earth complexes,[10-11] reduction, H abstraction, …). Thus, complex **2** appears as an ideal stable non-innocent platform, which can be generated in situ and used in several catalytic processes; we reported for example that **2** efficiently promoted alkyne [2+2+2] cycloadditions.[8]

In this report, we investigate more closely the coordination chemistry of the $(bcp^{\bullet-})_2Fe^{II}$ complex (**2**), with a particular focus on the dynamic ligand exchange that can be encompassed using this platform. An in-depth analysis of the ^{1}H NMR spectroscopic features of **2** are also discussed. Several reactivity patterns are discussed, such as the activation of organic electrophiles by electron transfer or the activation of alkyne compounds, as well as the role of Lewis acid additives than can help to control the formation of active species in catalytic processes by a modulation of the iron coordination sphere.

## 2. Results and discussion

### 2.1 ^{1}H NMR spectroscopy

The ^{1}H NMR spectrum of complex **2**, recorded in THF $d_8$ at 298 K, displays characteristic paramagnetic signals in the -90 / +120 ppm area (Figure 1a). This makes the ^{1}H NMR monitoring of the evolution of **2** straightforward when the latter is used as a catalyst in various transformations. However, the exact assessment of the chemical shifts observed for **2** is difficult on the sole basis of the ^{1}H NMR patterns (for example, scalar couplings are not always observed and broad signals may sometimes lead to inaccurate integrations). In this part, we used the temperature-dependence of those signals as well as theoretical modelling of the NMR spectrum to perform the assignment of the ^{1}H NMR signals.

The chemical shifts associated with those signals are temperature-dependent, as a consequence of the intrinsic paramagnetism of complex **2**. Indeed, the spinorbital population of a paramagnetic species by electrons, which are either parallel or antiparallel to the applied NMR magnetic field, strongly varies with the temperature. **2** thus adopts a paramagnetic behavior, its ^{1}H chemical shifts δ following a linear dependency with $T^{-1}$ in line with Curie's law (Figure 1b).
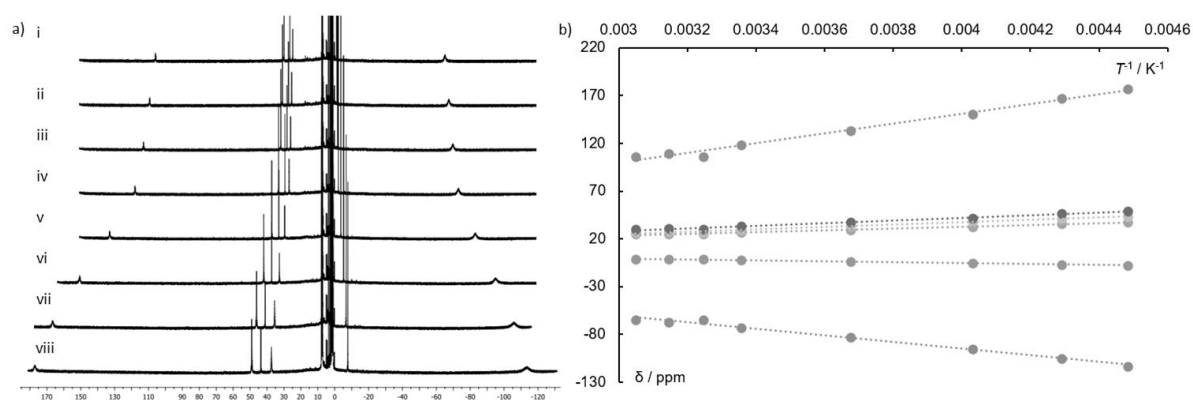


Figure 1: a) temperature-dependent ^{1}H NMR spectrum of **2** in THF $d_8$ (400 MHz) at i) 328 K, ii) 318 K, iii) 308 K, iv) 298 K, v) 272 K, vi) 248 K, vii) 233 K, viii) 223 K; data for the spectrum recorded at 298 K: 118.12 (s, 4H), 33.20 (s, 8H), 29.41 (s, 4H), 26.94 (s, 4H), -2.24 (s, 8H), -73.17 (bs, 12H); b) Curie plot ($\delta = f(1/T)$) for **2**.

No significant deviation to linearity in the Curie plot is observed in the temperature range investigated (223 to 328 K), attesting to the absence of any spin transition in solution in those conditions. Behavior

in solution thus seems to be similar to what some of us reported for the solid-state magnetic behavior of **2** analyzed by SQUID magnetometry.[8] Similarly, a linear Curie plot also attests to the monomeric nature of the paramagnetic complex in solution in the investigated temperature range; deviations to linearity are indeed observed when magnetically-coupled dimers are formed, as observed for the $Cr^{III}$ dinuclear complex [{$(C_5H_5)CrCl_2$}$_2$-μ(Cl,Cl)].[12]

However, it is interesting to note that all the NMR shifts of complex **2** do not follow strictly a Curie's law, which requests a linear relationship between δ and 1/T. In a pure Curie paramagnetic behavior, the chemical shifts intercept zero in linear 1/T plots. In complex **2**, strong deviations are observed, since all the $^1H$ chemical shifts exhibit a hyper-Curie behavior (see Figure S1). A hyper-Curie behavior is characterized by an intercept of the zero axis which is negative (resp. positive) for signals which display a positive (resp. negative) slope in the Curie plot.[13] Such a behavior usually attests to the presence of an excited state lying low in energy close to the ground state, and contributing to the physical properties of the complex. In order to rationalize the $^1H$ NMR spectrum of complex **2**, including the hyper-Curie paramagnetism as well as the origin of the chemical shifts observed experimentally, the electronic structure of the complex is investigated at density-functional theory (DFT) level.

In a paramagnetic complex, the NMR shifts $\delta_{exp}$ arise from the contribution of three terms: (i) the orbital shift $\delta_{orb}$, which takes into account the shielding of the analogue diamagnetic structure, (ii) the Fermi contact shift $\delta_{FC}$, which is due to the delocalization of the spin density along the chemical bonds in agreement with the symmetries of the molecular orbitals, and (iii) the dipolar pseudo-contact shift $\delta_{PC}$, which strongly depends on the distance between the NMR-active nucleus and the paramagnetic center:

$$\delta_{exp} = \delta_{orb} + \delta_{FC} + \delta_{PC}$$

In transition-metal paramagnetic complexes, the pseudo-contact term $\delta_{PC}$ is usually found to be negligible with respect to the Fermi contact shift $\delta_{FC}$.[14] Therefore, the two determining contributions are the orbital and Fermi contact shifts $\delta_{orb}$ and $\delta_{FC}$, which can be evaluated from theoretical calculations. For a system with a spin $S$, the Fermi contact shift is calculated according to the following equation:

$$\delta_{FC} = \frac{2\pi}{\gamma} g(iso) \mu(B) A \frac{S(S+1)}{3kT}$$

where $\gamma$ is the magnetogyric ratio of the considered nucleus, $g$(iso) the isotropic electron $g$ factor, $\mu(B)$ the Bohr magneton, $A$ the isotropic hyperfine coupling constant.[15]

The $T$-dependent $^1H$ NMR spectrum (VT-$^1H$ NMR) of **2** is computed within the PBE0 global-hybrid exchange-correlation approximation [16] (see SI for the corresponding references and computational details). In order to take into account the possible multiconfigurational description suggested by the experimental hyper-Curie NMR behavior, two triplet states were computed for complex **2** ($S = 1$). In line with experiments, the most stable one (ground state, **2$_{GS}$**) features an overall negative Mulliken spin density borne by the two bcp scaffolds ($\rho_{bcp,bcp}$ = -0.35) in an antiferromagnetic coupling with the metal ($\rho_{Fe}$ = +2.00). However, the computed VT-$^1H$ NMR spectrum of **2$_{GS}$** only partly fits with the experimental Curie plot (compare Figure 2a for the former and Figure 1b for the latter). In particular, no signal with a strong positive slope in the Curie plot is reproduced.
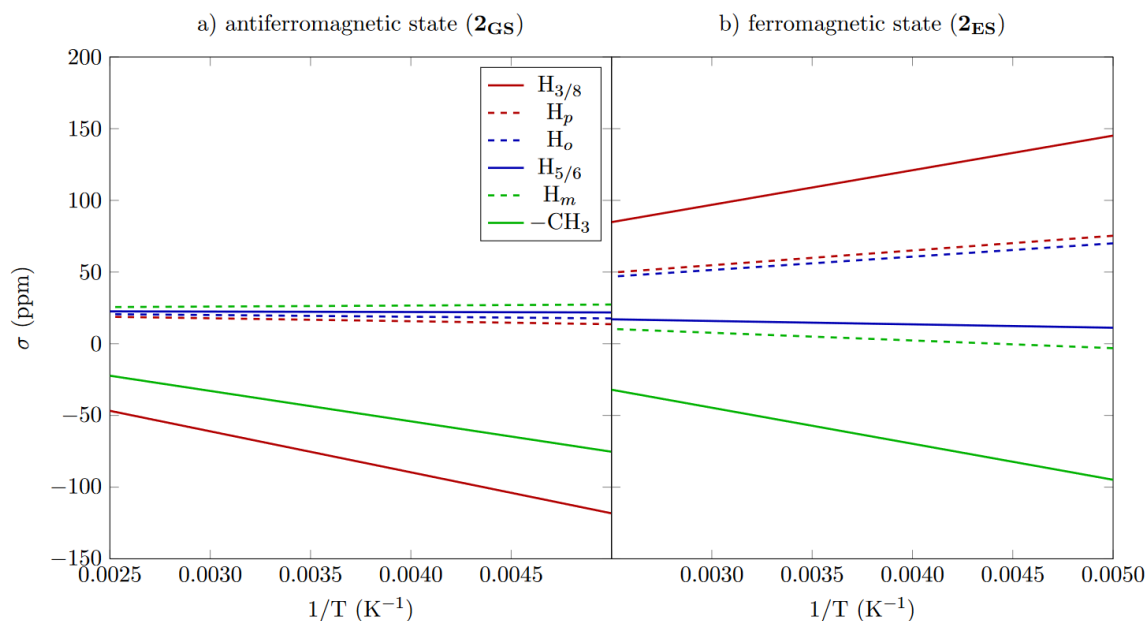
Figure 2: DFT-computed VT-$^1$H NMR spectra of triplet ($S = 1$) a) antiferromagnetic ground state $\mathbf{2_{GS}}$ and b) ferromagnetic excited state $\mathbf{2_{ES}}$.

On the other hand, a low-lying excited state $\mathbf{2_{ES}}$ is also localized 0.6 eV above $\mathbf{2_{GS}}$. This state is easily accessed, the 0.6 eV gap being smaller than the d-block span in **2** ($< 3$ eV). Unlike $\mathbf{2_{GS}}$, the excited triplet state $\mathbf{2_{ES}}$ is characterized by two ferromagnetically-coupled units ($\rho_{bcp,bcp} = +0.82$, and $\rho_{Fe} = +1.18$). However, the simulated VT-$^1$H NMR spectrum of $\mathbf{2_{ES}}$ correctly fits with experiments. Four shifts display a weak temperature dependence, and the two others are strongly affected with opposite slopes (compare Figures 2b and 1b). In other words, this suggests that the correct prediction of the $^1$H NMR shifts behavior of **2** requires to take into account two triplet states: the ground state $\mathbf{2_{GS}}$, featuring the experimentally characterized Fe / bcp$^{\bullet-}$ antiferromagnetic coupling, and an excited triplet state with a Fe / bcp$^{\bullet-}$ ferromagnetic coupling $\mathbf{2_{ES}}$, thus explaining why a hyper-Curie paramagnetism is observed on the experimental Curie plot (see SI for the detailed Mulliken spin density analysis).

Moreover, the good agreement between the simulated $T$-dependent $^1$H NMR spectrum of $\mathbf{2_{ES}}$ (Figure 2b) and the experimental spectrum also allows an accurate attribution of the experimental signals. The assessment of the $^1$H NMR signals of **2** is performed as a compromise between the integration curve of the experimental spectrum and DFT computations of the VT-$^1$H NMR spectrum of $\mathbf{2_{ES}}$ (Table 1).
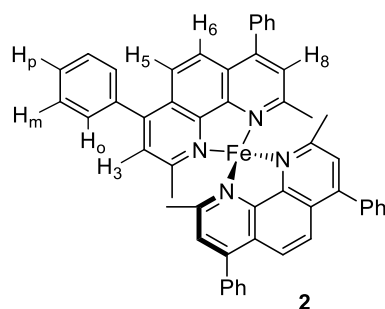
| δ (ppm) | Assignment |
|---|---|
| 118.12 (4H) | $H_{3/8}$ |
| 33.20 (8H) | $H_o$ |
| 29.41 (4H) | $H_p$ or $H_{5/6}$ |
| 26.94 (4H) | |
| -2.24 (8H) | $H_m$ |
| -73.17 (12H) | -CH$_3$ |

Table 1: assignment of the $^1$H chemical shifts of **2** (298 K) on the basis of the experimental spectrum and computed VT-$^1$H NMR spectrum of **2$_{ES}$**.

It is interesting to note that only protons in the $H_{3/8}$ and -CH$_3$ positions display an important thermal dependence (Figures 1b and 2b). As discussed above, the Fermi contact shift $\delta_{FC}$ is directly proportional to the isotropic hyperfine coupling constant $A$. The computed spectrum of **2$_{ES}$** (see Table S3) shows that the latter constants are particularly high for $H_{3/8}$ ($A_{H3/8}$ = -1.15 MHz) and -CH$_3$ protons ($A_{CH3}$ = 1.19 MHz). The other signals display isotropic hyperfine coupling constants lower than 0.5 MHz. This thus explains why the $H_{3/8}$ and -CH$_3$ slopes of the Curie plot are both important, and of opposite signs, the other shifts displaying more modest temperature dependences.

*2.2 Ligand exchange attempts starting from 2*

Given that the nature of non-innocent species can lead to complexes exhibiting a reactivity in-between their two extreme oxidation states, ligand substitution reactions involving complex **2** and classic Fe$^0$ or Fe$^{II}$ ligands possibly leading to heteroleptic (bcp)(L)Fe species were attempted (Scheme 2).
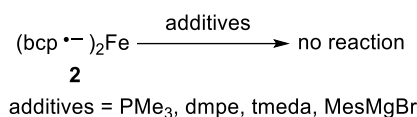


Scheme 2: attempts of ligand metathesis starting from **2**.

No ligand substitution was observed upon reaction of **2** with an excess (up to 10 equiv.) of neutral ligands such as PMe$_3$, 1,2-bis-dimethylphosphinoethane (dmpe) or N,N,N',N'-tetramethylethylenediamine (tmeda). The absence of neutral ligand exchange between **2** and those classic Fe$^{0/II}$ ligands demonstrates the strong non-innocent character of complex **2**, the metal-ligand interaction of which being dominated by the antiferromagnetic coupling between the reduced ligands L$^{•-}$ with the ferrous ion Fe$^{II}$. As a token of the strength of this interaction, no ligand exchange either occurred when **2** is treated by an excess of the Grignard reagent MesMgBr (Mes = 2,4,6-C$_6$H$_2$Me$_3$; 3 equiv. vs Fe). Displacement of anionic or neutral ligands bound to a Fe$^{II}$ center by MesMgBr usually easily yields the high-spin homoleptic *ate* complex [Mes$_3$Fe$^{II}$]$^-$ ($S$ = 2), which exhibits diagnostic resonances at δ = 131, 115 and 22 ppm in THF d$_8$ at 298 K.[17] This was for example reported by Bedford, who showed that (tmeda)-Fe$^{II}$ adducts afforded the sole complex [Mes$_3$Fe$^{II}$]$^-$ upon treatment by MesMgBr.[18] Therefore, the absence of

reactivity of complex **2** towards an excess of MesMgBr, noticeable for a complex which is accurately described by the $Fe^{II}$ oxidation state, attests to the strong metal / ligand interaction in **2**.

A second strategy which does not rely on a ligand substitution from **2** for the generation of heteroleptic (bcp)LFe complexes was also investigated. Complex $(bcp)Fe^{II}Cl_2$ (**1**) was reduced by two equivalents of a Grignard reagent (EtMgBr or $Me_2C=CHMgBr$) in the presence of several neutral ligands (Table 2). No new species was observed when tmeda was used (Entry 1), and **2** was the solely detected complex, likely formed by ligand comproportionation of elusive reduced (bcp)Fe intermediates. This is similar to what is observed when **1** is reduced in the absence of any additive: 50% of homoleptic complex $(bcp^{\bullet-})_2Fe^{II}$ (**2**) is detected along with 50% of ill-defined iron reduced nanoparticles.[8] Reduction of **1** in the presence of $PMe_3$ led to the detection of **2** with another paramagnetic species displaying ^{1}H NMR signals close to those of **2** and a silent ^{31}P NMR spectrum, suggesting that $PMe_3$ was involved in a paramagnetic complex. Although no further isolation of the latter could be performed, this suggests that heteroleptic scaffolds are more easily obtained by reduction of **1** in the presence of an exogenous ligand rather than by ligand metathesis using **2**. Reduction of **1** in the presence of one equivalent of another phen-derived ligand such as neocuproine (2,9-dimethyl-1,10- phenanthroline, ncp, Scheme 1a) led to the detection of 40% of the heteroleptic compound $(bcp^{\bullet-})(ncp^{\bullet-})Fe^{II}$ (**2"**), along with 50% of **2** and 10% of the bis-ncp complex $(ncp^{\bullet-})_2Fe^{II}$ (**2'**), Entry 3.

$$(bcp)Fe^{II}Cl_2 + L \quad \xrightarrow[\text{2 equiv. RMgBr}]{\text{THF, RT}} \quad (bcp)(L)Fe$$
$$\textbf{1}$$

| Entry | L | Iron species detected by ^{1}H NMR |
|-------|-----|-----------------------------------|
| 1 | tmeda | $(bcp^{\bullet-})_2Fe^{II}$ (**2**, 100%) |
| 2 | $PMe_3$ [a] | Mixture of $(bcp^{\bullet-})_2Fe^{II}$ (**2**) with another paramagnetic species |
| 3 | ncp [a] | $(bcp^{\bullet-})_2Fe^{II}$ (**2**, 50%) $(bcp^{\bullet-})(ncp^{\bullet-})Fe^{II}$ (**2"**, 40%) $(ncp^{\bullet-})_2Fe^{II}$ (**2'**, 10%) |

Table 2 : attempts for generating heteroleptic (bcp)(L)Fe complexes by reduction of **1** in the presence of L (1 equiv.); R = Et or $Me_2C=CH$; [a] see SI for NMR speciation.

In the latter case, the preference for the formation of the homoleptic bis-bcp complex $(bcp^{\bullet-})_2Fe^{II}$ (**2**) may be due to an easier electron transfer onto the bcp scaffold. For example, unsubstituted phen is slightly more difficult to reduce than its 4,7-$Ph_2$-*bis*-substituted analogue : $E_{red}(phen) = -2.53$ V *vs* $Fc^{0/+}$, and $E_{red}((4,7)\text{-}Ph_2\text{-}phen) = -2.39$ V *vs* $Fc^{0/+}$.[19] This trend would explain why the formation of a $Fe^{II}$-bound radical anion of bcp in complex **2** is favored compared to the formation of the heteroleptic species $(bcp^{\bullet-})(ncp^{\bullet-})Fe^{II}$ (**2"**).

It is also of note that radical anion $bcp^{\bullet-}$ could also directly be formed, and evidenced by X-band EPR spectroscopy (Figure 3, black line), upon treatment of bcp by one equivalent of $Me_2C=CHMgBr$, a Grignard reagent used to prepare **2** by reduction of **1** (Scheme 1b). Equimolar mixture of bcp and $Me_2C=CHMgBr$ leads to the detection of an isotropic signal centered at $g = 2.0037 \pm 0.0002$. The simulation of the hyperfine pattern (Figure 3, red line) fits with a $bcp^{\bullet-}$ radical delocalized onto two equivalent ^{14}N nuclei ($A_N = 7.2 \pm 0.1$ MHz = 0.26 mT) and two equivalent ^{1}H nuclei ($A_H = 7.2 \pm 0.1$

MHz = 0.26 mT). Another set of two equivalents $^1$H nuclei with smaller hyperfine coupling ($A_H' \approx 2$ MHz = 0.07 mT) was also taken into account in order to reproduce the global shape of the signal, the weakness of this coupling precluding however the detection of a more complex hyperfine pattern.
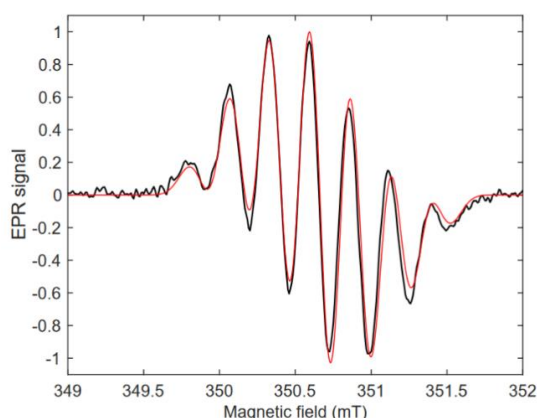


Figure 3: EPR spectrum (X-band, 298 K, THF:2-MeTHF 98:2) of a 1:1 mixture of bcp and Me$_2$C=CHMgBr (THF solution); black lines = experimental spectrum; red lines = simulation.

Formation of bcp$^{\bullet-}$ (possibly as a [(bcp)MgR]$^{\bullet}$ adduct) in those conditions likely proceeds by formation of a [(bcp)Mg(R)(Br)] precursor, in which an intramolecular electron transfer occurs, leading to the oxidation of the starting Grignard reagent, as reported by Kaim in the case of [(phen)MgR]$^{\bullet}$ adducts.[20] The hyperfine coupling constants in the simulated EPR spectrum given in Figure 3 moreover match with the hyperfine coupling constants of the [(phen)MgPh]$^{\bullet}$ radical reported by Kaim, which displays similar coupling constants of the radical with the $^{14}$N nuclei (0.290 mT), the $^1$H nuclei in C$_{3/8}$ positions of the phen ligand (0.290 mT), and the weakly coupled $^1$H nuclei at the C$_{5/6}$ positions (0.064 mT). Lei and Jutand also described similar phen-type radical anions formed by direct oxidation of $t$BuOK in a [(phen)KO$t$Bu] adduct.[7]

In the present case, formation of bcp$^{\bullet-}$ upon reaction of bcp and Me$_2$C=CHMgBr might also enhance the kinetics of the reduction of **1** into **2** (Scheme 1b). Indeed, preliminary studies by $^{57}$Fe-Mössbauer spectroscopy suggested that reduction of **1** with two equivalents of Me$_2$C=CHMgBr in the presence of one equiv. bcp proceeds within formation of a transient bis-hydrocarbyl (bcp)Fe$^{II}$(R)$_2$ intermediate, which affords complex **2** after reductive elimination of R-R.[8] However, given that radical anion bcp$^{\bullet-}$ is readily formed by oxidation of Me$_2$C=CHMgBr with bcp, it is not excluded that formation of **2** also involves one-electron transfers between bcp$^{\bullet-}$ and **1** as an alternative mechanism.

The interaction between the single-reduced bcp scaffolds and the Fe$^{II}$ ion being the key of the stability and redox properties of complex **2**, the reactivity of the latter in several elementary processes involving either alkynes or organic electrophiles has then been investigated.

*2.3 Activation of alkynes*

Some of us recently demonstrated that complex **2**, in situ generated by reduction of **1** by a Grignard reagent in the presence of one equiv. bcp, was an efficient catalyst for alkyne [2+2+2] cycloadditions, displaying a broad functional group tolerance (see example in Table 3).[8] From a mechanistic standpoint, the possible activation of an alkyne C≡C bond by **2** is intimately related to the available electronic density delocalized onto its bcp scaffolds. Indeed, no cycloaddition is observed when the ferrous precursor **1** is used in the absence of external reductant, demonstrating the requirement of a reduced complex for this transformation (Table 3, Entry 1). This result importantly shows that the

electronic density delocalized onto the ligands $L^{\bullet-}$ in **2** can be at play in the course of metallocentered processes, which require the presence of an iron center with a formal oxidation state lower than +II.
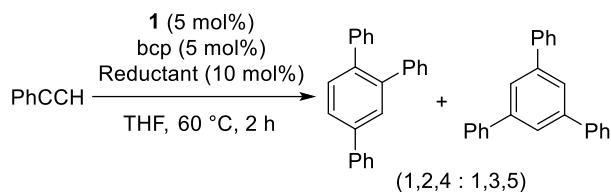


| Entry | Reductant | Residual salts present | Yield | 1,2,4 : 1,3,5 |
|-------|-----------|------------------------|-------|---------------|
| 1 | No reductant | - | 0 | - |
| 2 | $Me_2C=CHMgBr$ | $Mg^{II}$ salts | 98 | 99 : 1 |
| 3 | $KC_8$[a] | $K^I$ salts | 98 | 99 : 1 |
| 4 | $KC_8$[a] | Partial removal of $K^I$ salts by filtration | 89 | 99 : 1 |
| 5 | $KC_8$[a] | Full removal of $K^I$ salts by precipitation in cold toluene | 76 | 99 : 1 |
| 6 | $Me_2C=CHMgBr$ + 15-C-5 | (15-C-5)$Mg^{II}$ salts | 91 | 99 : 1 |

Table 3: effect of the presence of residual main-group salts on the phenylacetylene cycloaddition yield mediated by in situ generated **2**; [a] graphite was removed by filtration on a celite pad.

The redox duality between the $(bcp)_2Fe^0$ and $(bcp^{\bullet-})_2Fe^{II}$ descriptions of complex **2** is thus a key parameter of the reactivity of the latter, displacement of a neutral bcp ligand by a π-accepting ligand such as an alkyne leading to a $(bcp)Fe^0(\eta^2$-alkyne$)_2$ adduct being a first mandatory step of the cycloaddition process (Scheme 3). This ancillary ligand substitution at the formal $Fe^0$ stage is indeed the commonly admitted first step of the cycloaddition process, preceding the formation of a $Fe^{II}$ metallacycle by two-electron oxidative coupling of a reduced metal with two equivalents of alkyne.[21]
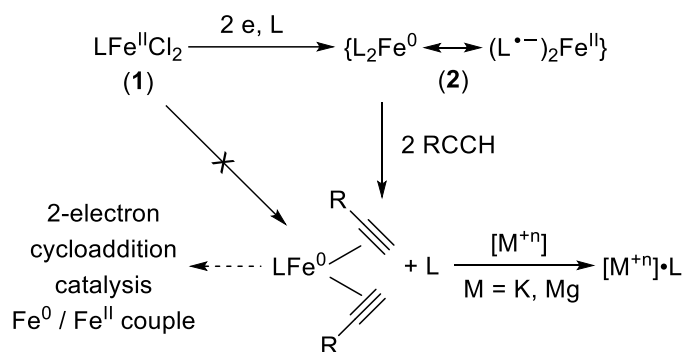


Scheme 3: dynamic ligand exchange assisted by main-group cations in alkyne [2+2+2] cycloaddition mediated by **2** as a precatalyst; L = bcp.
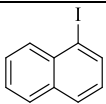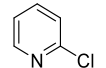
Interestingly, significant discrepancies were observed in the catalytic performances of **2** applied to phenylacetylene (PhCCH) cycloaddition, depending on the preparation of the catalyst (generation in situ or ex situ, with or without removal of residual salts, Table 3). When **2** is formed by reduction of **1** with 2 equiv. $Me_2C=CHMgBr$ in the presence of one equiv. bcp (method A), a near-quantitative 98% cycloaddition yield is obtained after 2 h at 60 °C (Table 3, Entry 2). Similarly, a 98% yield is obtained when **2** is formed by reduction of **1** with $KC_8$ in the same conditions (no elimination of $K^I$ salts, Table 1, Entry 3). However, when **2** is synthesized ex situ by reduction with $KC_8$ with a partial (Entry 4) or total (Entry 5, method B) elimination of the $K^I$ salts, a significant decrease in the cycloaddition yield is observed, since respectively 89% and 76% of cycloadduct are obtained in those conditions. Last, when **2** is generated using method A and subjected to addition of a classic $Mg^{II}$ crown-ether (15-C-5), a slight drop of the PhCCH cycloaddition yield is observed (91%, Entry 6).

In other words, the efficiency of **2** to act as a cycloaddition catalyst strongly depends on the presence of residual main-group cation salts such as $Mg^{II}$ or $K^I$ salts. When free $Mg^{II}$ or $K^I$ cations are present in the reaction medium (Entries 2-3), an almost quantitative cycloaddition occurs. On the other hand, when **2** is used as a purified, salt-free complex (prepared according to method B), less efficient cycloaddition performances are observed. Similarly, quenching the Lewis-acidity of the $Mg^{II}$ cation by formation of a (15-C-5)$Mg^{II}$ adduct also leads to more modest catalytic activity. Those experiments thus show that main-group Lewis acidic salts can be beneficial to the reaction outcome, thus pointing towards a synergy between the iron-centered activity and the $Mg^{II}$ or $K^I$ cation. Such cooperativity between iron catalysts and main-group reagents has been recently reported in a cross-coupling context, where the implication of $Zn^{II}$, $Mg^{II}$, $Li^I$ or $Al^{III}$ salts in the first or second iron coordination sphere proved to unlock key elementary steps of the coupling process.[22]

In the present case, owing to the strong metal-ligand interaction in $(bcp^{•-})_2Fe^{II}$, a key parameter of the success of the cycloaddition process is to trigger efficiently the decoordination of one bcp ligand to open the coordination sphere for the upcoming alkynes. In light of those results, this may be achieved by an electrophilic assistance of cationic $K^I$ or $Mg^{II}$ salts, which help to promote the decoordination of the bcp ligand by formation of a (bcp)$[M^{+n}]$ adduct (M = K, Mg, Scheme 3). Concomitantly, the electronic density borne by the bcp scaffold in $(bcp^{•-})_2Fe^{II}$ is relocalized onto the metal upon decoordination of bcp, affording formally reduced iron centers which can initiate the cycloaddition process.

*2.4 Electron Transfer reactivity*

Given that **2** formally contains 1-electron-reduced bathocuproine scaffolds ($bcp^{•-}$), the reactivity of this complex in electron-transfer processes with classic organic electrophiles was investigated. Single-Electron-Transfers (SETs) as well as concerted or stepwise two-electron processes are indeed key steps in a large variety of organic transformations involving organoiron intermediates, such as cross-couplings or C-H activations, and the nature of the reduction products formed consecutively to the electron transfer strongly depends on the nature of the reagents involved (reduction of a C-X into a C-H bond, reductive dimerization of a C-X bond into a C-C bond, …). Therefore, the reduction properties of **2** towards a variety of organic electrophiles has been examined (Table 4).

| Entry | R-X | $E_{red}$(R-X) (V *vs* SCE) [a] | Fe species detected by $^1H$ NMR | % R-X reduction products |
|---|---|---|---|---|
| 1 | | -1.92 | Complex mixture, full consumption of **2** | R-H (37) R-R (6) |
| 2 | | -2.37 | (bcp)$Fe^{II}Cl_2$ (**1**, 90%) $(bcp^{•-})_2Fe^{II}$ (**2**, 10%) | R-H (8) R-R (50) |

| 3 | [quinoline structure: N, Cl] | -1.92 | Complex mixture including **1, 2** (1:1 ratio) and 2,2'-bisquinoline-Fe$^{II}$ species | R-H (5) R-R (90) |
| 4 | [MeO–pyridine–Cl structure] | - | (bcp$^{•-}$)$_2$Fe$^{II}$ (**2**, 100%) | - (R-X recovered) |
| 5 | [2-bromobiphenyl structure, Br] | -2.4 [b] | (bcp$^{•-}$)$_2$Fe$^{II}$ (**2**, 100%) | - (R-X recovered) |
| 6 [c] | PhBCl$_2$ | - | (bcp)Fe$^{II}$Cl$_2$ (**1**, 100%) | Presumably formation of a borylene adduct |
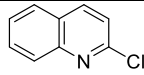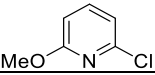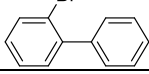
Table 4: analysis of the product distribution obtained upon stoichiometric reaction between **2** and 1 equiv. of an organic electrophile (R-X; conditions : 16 h at 20 °C in THF d$_8$); [a] see reference 23 (and references cited); [b] reduction potential of 4-bromobiphenyl, see reference 24; [c] in C$_6$D$_6$.

Partial reduction of 1-iodonaphthalene (1-NpI, Entry 1) is observed and 37% NpH are formed by reaction with **2**; traces of 1,1'-binaphthyl are detected. Formation of bisaryls by reductive coupling of heteroaryl chlorides is observed, since 2,2'-bipyridine (50%, Entry 2) and 2,2'-biquinoline (90%, Entry 3) are formed. Formation of those reduction products attests to an oxidation of **2** under those conditions; this is also in line with the $^1$H NMR monitoring of the reaction medium, which shows total (Entry 1) or partial (Entries 2-3) consumption of **2**, along with formation of **1** as an oxidation byproduct (Entries 2-3). On the other hand, less reactive substrates such as electron-rich 2-chloro-6-methoxypyridine and 2-bromobenzyl (Entries 4-5) are not affected by the presence of **2**, which remains unreacted. **2** also proved to efficiently reduce boron-based electrophiles, since treatment of **2** by 1 equiv. PhBCl$_2$ in C$_6$D$_6$ cleanly led to the formation of **1** as attested by $^1$H NMR (Figure S8), again in line with the 2-electron oxidation of **2**. However, the nature of the boron-containing product formed by reduction of PhBCl$_2$ is more difficult to assess. The low signal-to-noise ratio on the $^{11}$B NMR spectrum observed after addition of 0.5 and 1 equiv. PhBCl$_2$ on complex **2** strongly suggests that an important part of the starting material leads to a distribution of intractable products, which can correspond to either NMR-silent species or to a complex distribution of ill-defined diamagnetic compounds leading to broad signals. However, it is noteworthy that a broad singlet at δ($^{11}$B) = 22 ppm (C$_6$D$_6$) is detected under those conditions. A plausible hypothesis is that this signal may correspond to a reduction byproduct of PhBCl$_2$ featuring a diborene (RB=BR) moiety, which usually exhibits $^{11}$B NMR resonances in the 20-30 ppm area. This would be in line with the general procedure for the synthesis of Lewis-base-stabilized organic diborenes L•(R)B=B(R)•L, consisting of the treatment of a dihalogenoboron compound RBX$_2$ by a strong reductant such as Li in the presence of a Lewis base.[25,26] In the present case , the released bcp ligand may act, amongst other scenarios, as a stabilizing Lewis base to a PhB=BPh species formed after reduction of PhBCl$_2$.

The reductive properties of **2**, as outlined by the reduction of 1-iodonaphthalene, 2-heteroaryl chlorides or PhBCl$_2$, again demonstrate the availability of the electronic density localized onto the bcp scaffolds in (bcp$^{•-}$)$_2$Fe$^{II}$. No clear reactivity trend can be drawn between the reduction of the organic electrophiles used in Table 4 and their reduction potential. The most striking example is the drastic difference observed between 2-chloropyridine and 2-bromobiphenyl (Entries 2 and 5). These substrates have very close reduction potentials, but, whereas 2-bromobiphenyl is unreactive towards **2**, 2-chloropyridine affords 50% of 2,2'-bipyridine and 8% pyridine, formed by reduction of the starting C-Cl bond. The absence of correlation between the reactivity of the organic halides discussed in Table 4 towards **2** and their reduction potentials suggests that this reduction proceeds within a two-electron activation pattern.

The encouraging stoichiometric C-C bond formation by reductive coupling observed with heteroaryl chlorides (Entries 2-3) suggests that **2** can be involved in future catalytic processes for reductive

coupling of such substrates in mild conditions. This transformation would be particularly appealing taking into account the green chemistry principles, since the non-noble metal catalysis applied to this field is so far mostly dominated by the use of nickel-based catalysts.[27] As a proof of concept of the ability of **2** to catalyze reductive coupling transformations, 2-chloroquinoline could be transformed with an appreciable 90% yield into 2,2'-biquinoline using **2** as a catalyst (10 mol%) and $Mg^0$ turnings (2 equiv.) as a sacrificial reductant (Scheme 4) in mild conditions (16 h, room temperature). No conversion of the starting material occurred in the presence of $Mg^0$ alone (that is, in the absence of **2**).
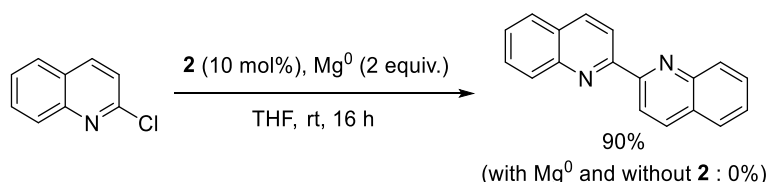


Scheme 4: reductive coupling of 2-chloroquinoline catalyzed by **2** in the presence of $Mg^0$ as a reductant.

From a mechanistic standpoint, reductive coupling of aryl chlorides can rely on sequential oxidative additions, as reported by Lautens for $Ni^0$-catalyzed couplings,[27] amongst other examples.[28,29,30] In the system reported by Lautens, a $Ni^0$ / $Ni^{II}$ / $Ni^{I}$ / $Ni^{III}$ sequence is suggested. Inspired by this work, a tentative mechanism for the reductive homocoupling of 2-chloroquinoline catalyzed by **2** has been proposed (Scheme 5). A first oxidative addition of **2** onto the C-Cl bond leads to an intermediate heteroaryl-$Fe^{II}$ species **A**.
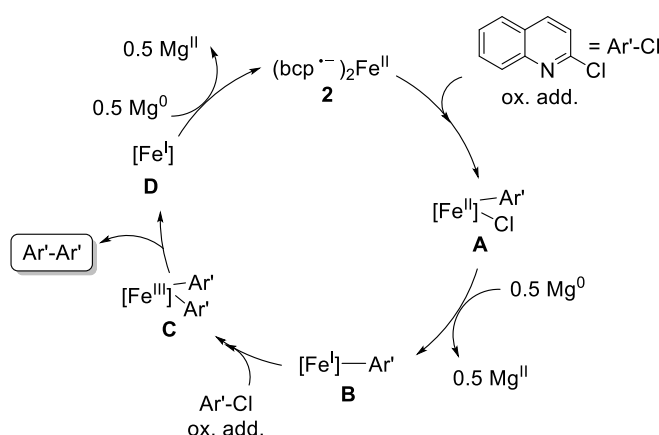


Scheme 5: tentative catalytic cycle for the reductive coupling catalyzed by **2**.

**A** is reduced by $Mg^0$ (0.5 equiv.) into a heteroaryl-$Fe^{I}$ intermediate **B**, which promotes the second oxidative addition onto the electrophile to afford a bis-heteroaryl-$Fe^{III}$ species **C**. Reductive elimination of the C-C bond at the latter affords the expected coupling product, along with a $Fe^{I}$ complex **D**, which is reduced by $Mg^0$ (0.5 equiv.) to lead back to **2**, closing the catalytic process. Moreover, it is not excluded that the $Mg^{II}$ salts generated at each catalytic cycle play an important role in the reductive coupling mechanism, in line with the Ni-based system developed by Lautens which requires the use of $MgCl_2$ as an additive.

A key step of the mechanism discussed in Scheme 5 is thus the promotion of the second oxidative addition involving the singly-reduced intermediate **B** (which is at a formal $Fe^{I}$ oxidation state assuming that no ligand non-innocence affects this assignment). Feasibility of this step has been probed using an aryl halide (herein PhI) and a singly-reduced (bcp)FeX platform generated by cyclic voltammetry from (bcp)$Fe^{II}Cl_2$ (**1**). **1** is characterized by a reversible one-electron reduction peak at $E_{p,R1}$ = -1.68 V *vs* $Fc^{0/+}$, associated with oxidation peak at $E_{p,O1}$ = -1.61 V *vs* $Fc^{0/+}$ (Figure S9, $\Delta E_p$ = 70 mV). A singly-reduced species (bcp)FeCl (either described as (bcp)$Fe^{I}Cl$ or as (bcp$^{•-}$)$Fe^{II}Cl$) is thus likely formed at this

potential (Figure 4a). A second reduction peak at $E_{p,R2}$ = -2.45 V $vs$ Fc$^{0/+}$ can be observed (Figure 4b, yellow lines). This non-reversible peak can be associated with the reduction of (bcp)FeCl generated at R$_1$ in non-active iron nanoparticles, explaining the full lack of reversibility on the reverse scan.



Figure 4: a) redox events observed upon the reduction of **1** in the absence or the presence of PhI; b) cyclic voltammetry of **1** in the absence (yellow lines) or the presence (orange lines) of 1 equiv. PhI, recorded in DMF, at 20°C, at a scan rate of 0.25 V.s$^{-1}$ in the presence of 0.1 M [$n$-Bu$_4$N][PF$_6$] as a supporting electrolyte.

When the same cyclic voltammetry is run in the presence of one equiv. PhI per mole of **1**, reduction of **1** is still observed at R$_1$, and a new reduction peak develops at $E_{p,R3}$ = -1.94 V $vs$ Fc$^{0/+}$ (Figure 4b, orange lines). This suggests that species (bcp)FeCl, generated at R$_1$ in the diffusion layer of the electrode, reacts with PhI. Since no catalytic current is observed at R$_1$, no SET occurs between those two species, since it would regenerate complex **1** and thus lead to an increase of the current peak at R$_1$. Formation of a new well-defined species reduced at R$_3$ is thus in line with an oxidative addition of (bcp)FeCl into the C-I bond of PhI, leading to an organoiron(III) intermediate (Figure 4a). **1** is partly reaffored by reduction of the latter on the reverse scan, as attested by the increase of O1 oxidation peak (Figure 4a-b). Overall, this result supports the reductive coupling mechanism discussed in Scheme 5.


## Conclusion

In this report, we demonstrate that the ligand dynamics in non-innocent complex (bcp$^{•-}$)$_2$Fe$^{II}$ (**2**) is mostly driven by the strong coupling between the reduced bcp ligand and the Fe$^{II}$ ion, precluding easy ligand exchange at the Fe$^{II}$ stage. The coupling between the ligand- and metal-localized electronic densities is reflected by both hyper-Curie thermal-dependence of the NMR signals of **2** along with the corresponding DFT simulations. However, strongly π-accepting substrates such as alkynes can induce a Fe$^0$-like behavior in **2** and lead to [2+2+2] cycloadditions, in synergistic interaction with main-group salts ensuring an efficient modulation of the iron coordination sphere in the cycloaddition process. The promising reactivity of **2** in reductive coupling catalysis moreover paves the way to the development of

iron-based methods for carrying out such transformations as a greener alternative to the current state-of-the-art.

## Acknowledgements

## References

[1] A. Bencini, V. Lippolis, 1,10-Phenanthroline: A versatile building block for the construction of ligands for various purposes, Coord. Chem. Rev. 254 (2010) 2096-2180, doi:10.1016/j.ccr.2010.04.008.

[2] P.G. Sammes, G. Yahioglu, 1,10-Phenanthroline: a versatile ligand, Chem. Soc. Rev. 23 (1994) 327-334, doi:10.1039/CS9942300327.

[3] P. Alreja, N. Kaur, Recent advances in 1,10-phenanthroline ligands for chemosensing of cations and anions, RSC Adv. 6 (2016) 23169-23217, doi:10.1039/C6RA00150E.

[4] S.C. Bart, E. Lobkovsky, P.J. Chirik, Preparation and Molecular and Electronic Structures of Iron(0) Dinitrogen and Silane Complexes and Their Application to Catalytic Hydrogenation and Hydrosilation, J. Am. Chem. Soc. 126 (2004) 13794–13807, doi:10.1021/ja046753t.

[5] K.T. Sylvester, P.J. Chirik, Iron-Catalyzed, Hydrogen-Mediated Reductive Cyclization of 1,6-Enynes and Diynes: Evidence for Bis(Imino)Pyridine Ligand Participation, J. Am. Chem. Soc. 131 (2009) 8772–8774, doi:10.1021/ja902478p.

[6] T.K. Mukhopadhyay, R.K. Feller, F.N. Rein, N.J. Henson, N.C. Smythe, R.J. Trovitch, J.C. Gordon, Chem. Commun. 48 (2012) 8670-8672, doi:10.1039/C2CC33926A.

[7] H. Yi, A. Jutand, A. Lei, Evidence for the interaction between tBuOK and 1,10-phenanthroline to form the 1,10-phenanthroline radical anion: a key step for the activation of aryl bromides by electron transfer, Chem. Commun. 51 (2015) 545-548, doi:10.1039/C4CC07299E.

[8] M. Féo, N.J. Bakkas, A. Radovic, W. Parisot, A. Clisson, L.-M. Chamoreau, M. Haddad, V. Ratovelomanana-Vidal, M.L. Neidig, G. Lefèvre, Thermally Stable Redox Noninnocent Bathocuproine-Iron Complex for Cycloaddition Reactions, ACS Catal. 13 (2023) 4882–4893, doi:10.1021/acscatal.3c00353.

[9] K.A. Jesse, A.S. Filatov, J. Xie, J.S. Anderson, Neocuproine as a Redox-Active Ligand Platform on Iron and Cobalt, Inorg. Chem. 58 (2019) 9057-9066, doi:10.1021/acs.inorgchem.9b00531.

[10] G. Nocton, W.L. Lukens, C.H. Booth, S.S. Rozenel, S.A. Melding, L. Maron, R.A. Andersen, Reversible Sigma C–C Bond Formation Between Phenanthroline Ligands Activated by (C5Me5)2Yb, J. Am. Chem. Soc. 136 (2014) 8626-8641, doi:10.1021/ja502271q.

[11] G. Nocton, L. Ricard, Reversible C–C coupling in phenanthroline complexes of divalent samarium and thulium, Chem. Commun. 51 (2015)3578-3581, doi:10.1039/C5CC00289C.

[12] P. Fernandez, H. Pritzkow, J.J. Carbo, P. Hofmann, M. Enders, ^{1}H NMR Investigation of Paramagnetic Chromium(III) Olefin Polymerization Catalysts: Experimental Results, Shift Assignment and Prediction by Quantum Chemical Calculations, Organometallics 26 (2007) 4402-4412, doi:10.1021/om070173y.

[13] L. Banci, I. Bertini, C. Luchinat, R. Pierattelli, N.V. Shokhirev, F.A. Walker; Analysis of the Temperature Dependence of the 1 H and 13C Isotropic Shifts of Horse Heart Ferricytochrome c: Explanation of Curie and Anti-Curie Temperature Dependence and Nonlinear Pseudocontact Shifts in a Common Two-Level Framework, J. Am. Chem. Soc. (1998), 120, 8472-8479, doi:10.1021/ja980261x.

[14] Solution NMR of Paramagnetic Molecules: Applications to Metallobiomolecules and Models, ed. I. Bertini, C. Luchinat and G. Parigi, Elsevier, Amsterdam, 2001.

[15] A. Borgogno, F. Rastrelli, A. Bagno, Predicting the spin state of paramagnetic iron complexes by DFT calculation of proton NMR spectra, Dalton Trans. 43 (2014) 9486-9496, doi:10.1039/C4DT00671B.

[16] C. Adamo, V. Barone, Toward reliable density functional methods without adjustable parameters: The PBE0 model, J. Chem. Phys. 110 (1999) 6158–6170, doi:10.1063/1.478522; M. Ernzerhof; G.E. Scuseria, Assessment of the Perdew–Burke–Ernzerhof exchange-correlation functional, J. Chem. Phys. 110 (1999) 5029–5036, doi:10.1063/1.478401.

[17] L. Rousseau, C. Herrero, M. Clémancey, A. Imberdis, G. Blondin, G. Lefèvre, Evolution of Ate-Organoiron(II) Species towards Lower Oxidation States: Role of the Steric and Electronic Factors, Chem. Eur. J. 26 (2020) 2417-2428, doi:10.1002/chem.201904228.

[18] R.B. Bedford, P.B. Brenner, E. Carter, P.M. Cogswell, M.F. Haddow, J.N. Harvey, D.M. Murphy, J. Nunn, C.H. Woodall, TMEDA in Iron-Catalyzed Kumada Coupling: Amine Adduct versus Homoleptic "ate" Complex Formation, Angew. Chem. Int. Ed. 53 (2014) 1804-1808, doi:10.1002/anie.201308395.

[19] H. Ferreira, M.M. Conradie, K.G. von Eschwege, J. Conradie, Electrochemical and DFT study of the reduction of substituted phenanthrolines, Polyhedron, 122 (2017) 147-154, doi:10.1016/j.poly.2016.11.018.

[20] W. Kaim, Electron transfer to 1,10-phenanthroline by grignard reagents. the spin distribution in organomagnesium radical complexes, J. Organomet. Chem. 222 (1981) C17-C20, doi:10.1016/S0022-328X(00)89165-2.

[21] A. Roglans, A. Pla-Quintana, M. Solà, Mechanistic Studies of Transition-Metal-Catalyzed [2 + 2 + 2] Cycloaddition Reactions, Chem. Rev. 121 (2021) 3 1894–1979, doi.org/10.1021/acs.chemrev.0c00062.

[22] V. Wowk, G. Lefèvre, The crucial and multifaceted roles of main-group cations and their salts in iron-mediated cross-couplings, Dalton Trans. 51 (2022) 10674-10680, doi:10.1039/D2DT00871H.

[23] R.J. Enemaerke, T.B. Christensen, H. Jensen, K. Daasbjerg, Application of a New Kinetic Method in the Investigation of Cleavage Reactions of Haloaromatic Radical Anions, J. Chem. Soc., Perkin Trans. 2 (2001) 1620-1630, doi:10.1039/B102835A.

[24] N.G.W Cowper, C.P. Chernowsky, O.P. Williams, Z.K. Wickens, Potent Reductants via Electron-Primed Photoredox Catalysis: Unlocking Aryl Chlorides for Radical Coupling, J. Am. Chem. Soc. 142 (2020) 2093-2099, doi:10.1021/jacs.9b12328.

[25] H. Braunschweig, R.D. Dewhurst, Boron–Boron Multiple Bonding: From Charged to Neutral and Back Again, Organometallics 33 (2014) 6271-6277, doi:10.1021/om500875g.

[26] P. Bissinger, H. Braunschweig, A. Damme, T. Kupfer, A. Vargas, Base-Stabilized Diborenes: Selective Generation and $\eta^2$ Side-on Coordination to Silver(I), Angew. Chem. Int. Ed. 51 (2012) 9931-9934, doi:10.1002/anie.201204449.

[27] B. Mirabi, A.D. Marchese, M. Lautens, Nickel-Catalyzed Reductive Cross-Coupling of Heteroaryl Chlorides and Aryl Chlorides, ACS Catal. 11 (2021) 20 12785–12793, doi.org/10.1021/acscatal.1c02307.

[28] S. Nunomoto, Y. Kawakami, Y. Yamashita, Cross-coupling reaction of 2-(1,3-butadienyl)magnesium chloride with alkyl or aryl halides by lithium chloride-cupric chloride (Li2CuCl4), a superior catalyst, J. Org. Chem. 48 (1983), 1912–1914, doi.org/10.1021/jo00159a028.

[29] M. Fujita, H. Oka, K. Ogura, Palladium(0)/LiCl promoted cross-coupling reaction of (4-pyridyl)stannanes and aromatic bromides: Easy access to poly(4-pyridyl)-substituted aromatics, Tet. Lett. 36 (1995), 5247-5250, doi.org/10.1016/0040-4039(95)00983.

[30] L. Huang, L.K.G. Ackerman, K. Kang, A.M. Parsons, D.J. Weix, LiCl-Accelerated Multimetallic Cross-Coupling of Aryl Chlorides with Aryl Triflates, J. Am. Chem. Soc. 141 (2019), 10978–10983, doi.org/10.1021/jacs.9b05461.